Original Research Article

International Journal of
Protective Structures

A numerical investigation of blast-structure interaction effects on primary blast injury risk and the suitability of existing injury prediction methods

International Journal of Protective Structures
2022, Vol. 0(0) 1–20

DOI: 10.1177/20414196221136157
journals.sagepub.com/home/prs

Jack Denny[1], Genevieve Langdon[2], Sam Rigby[2], Alex Dickinson[3] and James Batchelor[4]

Abstract

Explosions increasingly occur in densely populated, urban locations. Primary blast injuries (PBIs), caused by exposure to blast wave overpressure, can be predicted using injury criteria, although many are based on idealised loading scenarios that do not necessarily reflect real life situations. At present, there is limited understanding of how, and to what extent, blast-structure interaction influences injury risk, and the suitability of injury criteria that assume idealised loading. This work employed computational fluid dynamics to investigate the influence of blast interaction effects such as shielding and channelling on blast load characteristics and predicted PBIs. The validated modelling showed that blast interaction with common urban features like walls and corners resulted in complex waveforms featuring multiple peaks and less clearly defined durations, and that these alter potential injury risk maps. For example, blast shielding due to corners reduced peak overpressures by 43%–60% at locations behind the corner. However, when the urban layout included a corner and a wall structure, higher pressures and impulse due to channelling were observed. The channelling significantly increased the injury risk at the exposed location and reduced the shielding effects behind the corner. In these cases, the application and interpretation of existing injury criteria had several limitations and reduced reliability. This demonstrates that structural-blast interaction from common urban layouts has a significant effect on PBI risk. Specific challenges and further work to develop understanding and reliability of injury prediction for urban blast scenarios are discussed.

[1]Department of Civil Engineering, Faculty of Engineering and Physical Sciences, University of Southampton, UK
[2]Department of Civil and Structural Engineering, University of Sheffield, UK
[3]Department of Mechanical Engineering, Faculty of Engineering and Physical Sciences, University of Southampton, UK
[4]Clinical Informatics Research Unit, Faculty of Medicine, University of Southampton, UK

Corresponding author:
Dr. Jack Denny, Department of Civil Engineering, University of Southampton, Boldrewood Innovation Campus, Burgess Rd, Southampton SO16 7QF, UK.
Email: Jack.Denny@soton.ac.uk

Keywords
blast-structure interaction, built environment, injury criteria, numerical analysis, computational fluid dynamics, injury prediction, blast effects

Introduction

Explosions are a rapid release of a large quantity of energy in a short period of time (typically microseconds), resulting in a high-temperature fireball and high-pressure blast waves travelling at supersonic velocities, propagating into the surrounding environment (Kinney and Graham, 1985). Explosions increasingly occur in densely populated locations due to the shifting nature of conflict into urban areas, terrorist attacks and industrial accidents such as the 2020 Beirut blast (Rigby et al., 2020). These can result in devastating injuries, with so-called 'primary' blast injuries (PBIs) caused by exposure to the blast wave overpressure (US Department of Defense (DoD), 2006). Data from Action on Armed Violence has shown that when explosive weapons are used in towns and cities, 91% of casualties are civilians (Action on Armed Violence (AOAV), 2020).

Urban environments comprise a large variety of geometries and layouts that can significantly alter the explosion effects and resulting blast injuries. Blast wave interaction in urban environments leads to reflection, shielding and channelling and in closed spaces, blast waves can reflect, ricochet and coalesce (Champion et al., 2009). Some of these individual physical mechanisms might be beneficial (e.g. shielding) while others are detrimental to the safety of people and infrastructure. Blast wave reflections from rigid surfaces, for example, are known to magnify the overpressures many times over (Ben-Dor, 2007). Analysis of the 2004 Madrid Train Bombings demonstrated that confinement of explosions resulted in more serious injury outcomes (Peters, 2011). At larger scales, analysis of the 2020 Beirut explosion demonstrated shielding and channelling effects caused by high-rise buildings (Valsamos et al., 2021). The interaction between the aforementioned mechanisms is complex (Drazin, 2017; Johnson et al., 2022), however, it is clear from real-life events that explosions in urban areas lead to more deaths and injuries overall.

Blast propagation and interaction phenomena with obstacles arising in urban and complex landscapes can be studied using modelling tools such as computational fluid dynamics (Drazin, 2017; Johnson et al., 2022; Noorpoor et al., 2020; Remennikov and Rose, 2005; Valsamos et al., 2021). Models can be developed for specified blast scenarios, permitting examination of a wide range of blast effects at different scales, from individual buildings to broader cityscapes, at varying fidelities and sophistication. Modelled blast loading parameters can potentially then be used to estimate blast injury risk or the expected spatial extent of casualties by referring to injury criteria.

Multiple criteria for primary blast injury (PBI) have been proposed to predict injury outcomes on a probabilistic basis depending on the blast conditions a person is exposed to. These criteria have multiple forms with different input and output parameters, applicability and assumptions. The most widely reported criteria are applicable to idealised blast waves, or 'Friedlander' type waveforms (Friedlander, 1946) that develop in open-field explosion scenarios. For example, the Bowen curves (Bowen et al., 1968), which despite being over 50 years old are still widely used as the standard for blast pulmonary injury prediction. Alternative injury models have also been developed with applicability to non-ideal and complex blast waveforms, such as the Axelsson BTD model (Axelsson and Yelverton, 1996), which accounts for injuries to the respiratory tract, the thorax and the abdominal area, and the Weathervane SP model (Li et al., 2008), reviewed in greater detail by Teland (2012). These models allow the input of non-ideal blast waves and predict injury in terms of an 'Adjusted Severity of Injury Index'. These models have increased complexity and their accuracy is unknown in

comparison to the injury criteria based on idealised blast wave inputs, with Teland suggesting that Axelsson-based methods are underpinned by poor quality data (Teland, 2012). As reviewed by Denny et al. (2021a), there still lacks consensus on the reliability, applicability and underlying assumptions of certain PBI criteria. As a result, injury criteria based on idealised (open-field) blast waveforms remain widely adopted and more suitable for fast-running injury risk estimations.

It is widely understood that urban environments can modify blast loading (Drazin, 2017; Johnson et al., 2022; Smith and Rose, 2002, 2006) and researchers have examined how some of these affect structures (Chaudhary et al., 2019; Hao et al., 2016). However, the consequences of the altered blast loading characteristics for potential blast injury at different locations within the urban environment is not well understood. Furthermore, the ability to model injury risk for urban blast scenarios, and in particular, the suitability of applying injury criteria based on ideal assumptions has not yet been analysed. These knowledge gaps are increasingly important as researchers modelling urban blast scenarios with high levels of sophistication seldom question the validity and applicability of injury criteria for predicting the spatial extent of blast injuries. This paper begins to address how, and to what extent, modified blast loading characteristics influence the risk of PBI. The challenges and limitations of using injury criteria based on idealised blasts should also be explored, with a view to distinguish the problematic features of blast waveforms for predicting injury risk.

This paper presents computational fluid dynamics (CFD) simulations of explosive events where the loading is influenced by typical urban features such as walls and corners, and shows how these features change the characteristics of blast pressure loads through the locality. The CFD analysis is validated using experimental data from Gajewski and Sielicki (2020) on the effects of corners on blast overpressure and specific impulse histories, and extends this numerically to consider the influence of a wall and the channelling effects it has on blast loading and injury risk. The paper then uses the simulated loading characteristics at certain locations to ascertain the influence of building geometry on expected PBIs and then assesses the suitability and limitations of using openly available injury criteria. This work will be useful to researchers, engineers, health professionals, urban planners and emergency response planning teams in appreciating how building features can adversely affect PBI arising from an explosive event in urban environments.

Methodology

Overview

The experimental work by Gajewski and Sielicki (2020) was used to validate the CFD model that analyses structural-blast interaction effects resulting from an explosive detonating near a rigid building corner (Figure 1). Gajewski and Sielicki (2020) investigated blast interaction and shielding effects provided by a rigid building corner, examining blast waves from the detonation of brick-shaped 200 g and 400 g TNT charges. Overpressure histories were measured at four locations around the corner structure.

In this paper, CFD analyses were undertaken to model blast wave interaction with a corner geometry resulting from the detonation of a 400 g TNT charge. Two additional series of CFD analyses modelled the same explosive detonation, though examined two different scenarios: (1) without the corner structure to examine the free-field blast propagation scenario, and (2) with the corner structure and an additional wall (running along the entire length of the bottom of the domain, i.e. $y = 0$, as in Figure 2) to examine channelling effects. The free-field scenario was modelled as opposed to using semi-empirical relations (Hyde, 1991, 1992; Kingery and Bulmash, 1984) in order to resolve ground reflection effects. Comparison between the three urban layouts enabled the extent

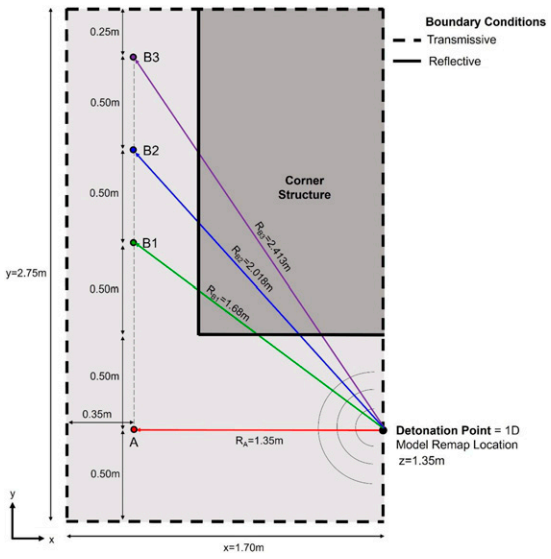

Figure 1. Plan view schematic of the corner modelling scenario, detonation point and pressure monitoring locations at a height z = 1.35 m above the ground surface.

that overpressure histories were modified by interaction with the corner (and additional wall) to be obtained, so that the corresponding influence on PBI risk could be studied.

Overpressure histories were measured at four locations (A, B1-B3) surrounding the rigid corner structure (Figure 1) consistent with Gajewski and Sielicki (2020). Gauge A was positioned in direct line-of-sight of the detonation. Gauges B1, B2 and B3 were located at successive distances around the corner to examine the blast shielding effects of the rigid corner (Figure 1). The detonation point and pressure gauges were positioned at height z = 1.35 m above the ground surface. This height represented the chest centre for a standing position, or the eardrums for an aiming-kneeling position, for a medium-sized person (Gajewski and Sielicki, 2020).

Primary blast injury risk was interpreted at each gauge location through inspection of blast wave parameters and with reference to pre-defined injury criteria, based on more detailed reviews by Denny et al. (2021a, 2021b). Primary blast injury risk profiles were grouped according to area of the body affected: (1) the auditory system, (2) pulmonary injury and risk of lethality, and (3) brain-related PBI (Table 1).

Numerical modelling methodology

Computational fluid dynamics is a numerical method used to simulate the propagation of fluid through a domain and around objects. Fluid dynamics are the fundamental physical equations underpinning CFD and are based on the continuity, momentum and energy equations, known as the Navier–Stokes equations (Anderson, 2009; Mays and Smith, 1995; Smith and Hetherington, 1994). Simplifications of the Navier–Stokes equations, where the fluid is assumed to be 'inviscid' in which the kinematic and dynamic viscosity, μ and ν are zero, are known as the Euler equations, which represent the conservation of mass (continuity), momentum and energy. Many proprietary CFD

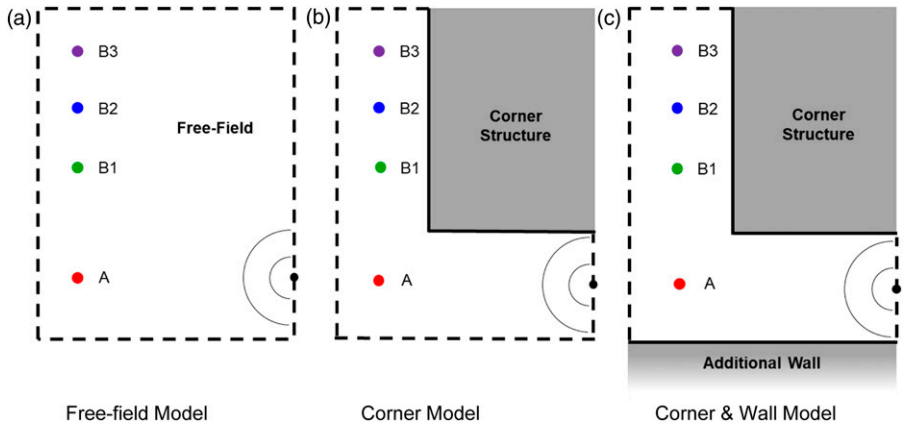

Figure 2. Plan view schematics of each blast scenario modelled. (a) Free-field Model, (b) Corner Model, (c) Corner & Wall Model.

Table 1. Summary of primary blast injury (PBI) criteria used to assess PBI risk.

Blast injury area	Criteria description
Auditory system	Peak overpressure thresholds • 35 kPa (US Department of Defense (DoD), 2008) – Threshold for eardrum rupture • 103 kPa (US Department of Defense (DoD), 2008) – 50% probability of eardrum rupture • 202 kPa (Jensen and Bonding, 1993) – 100% probability of eardrum rupture
Pulmonary injury & lethality	Peak overpressure-positive phase duration functions Bowen curves (Bowen et al., 1968) for pulmonary (lung) blast injuries assuming a 70 kg man stood near a wall, including: • Threshold for pulmonary blast injury • 1%, 50% and 99% probability of fatality
Brain-related primary blast injury	Peak overpressure thresholds • 144 kPa (Rafaels et al., 2012) – 50% risk of mild brain haemorrhage

programs or 'hydrocodes' with shock wave modelling capabilities are based on solving these inviscid Euler equations.

ANSYS Autodyn (ANSYS, 2020) (Version 2020 R2) was used to perform CFD analyses in a two-stage approach. Firstly, the one-dimensional (1D) detonation of a 400 g spherical TNT charge was modelled as a free-air explosion for the early-stage blast wave propagation, that is, up to a stand-off distance, $R < 0.5$ m. Secondly, three-dimensional (3D) inviscid Eulerian CFD analyses 're-mapped' the 1D incident blast wave to propagate within the domain to interact with the corner geometry (and wall), including blast reflections at the corner walls and ground surface.

Detonation & near-field (R < 0.5 m) blast propagation (1D model). The explosive was modelled as a sphere, as opposed to a cuboid in the experimental work, to facilitate the use of 1D simulations in the early blast propagation stages. Charge shape effects have been shown to have minimal influence on

specific impulse beyond a scaled distance of 2.64 m/kg$^{1/3}$ (Sherkar et al., 2010, 2016), however, for lower scaled distances, that is, at gauges A and B1, lower peak overpressures and specific impulses can be expected for the spherical charge. The primary reason for using the work of Gajewski and Sielicki (2020) for validation was to verify that the corner model generated similar trends before examining the influence of the additional wall and corresponding injury risk, therefore the spherical charge simplification was deemed valid for this study.

A radially symmetric 1D wedge domain was used to model detonation and subsequent blast wave propagation in air, to a distance of 0.5 m corresponding to the blast wave propagation to the nearest reflective surface, the wall (Figure 1). A wedge domain of length, L = 2.0 m was necessary to provide sufficient space to capture the entire blast wave history to evaluate impulse. TNT material was specified at the tip of the wedge domain containing elements of atmospheric air, such that the explosion and resulting shockwave propagated towards the open end (Figure 3). An 'outflow' boundary condition was assigned to the distal end to allow air to exit after being accelerated by the shock wave, although the simulation was terminated before end expansion waves had reached the gauge location.

Default values for the TNT and air equations of state (EOS) were used in the computations and retrieved from the standard Autodyn library (Table 2). The Jones–Wilkins–Lee (JWL) EOS (Dobratz and Crawford, 1985; Lee et al., 1968) was used to model the TNT material (equation (1))

$$p = A\left(1 - \frac{\omega}{R_1 V}\right)e^{-R_1 V} + B\left(1 - \frac{\omega}{R_2 V}\right)e^{-R_2 V} + \frac{\omega}{V}e \tag{1}$$

In equation (1), p denotes pressure and V and e are the specific volume and specific internal energy of the explosive, respectively. Parameters A, B, R_1, R_2 and ω are constants that can be evaluated through experiments for any high explosive material. For the TNT material, values for these parameters were taken from the Autodyn built-in material library and listed in Table 2.

Air was modelled using the ideal gas EOS (equation (2))

$$p = (\gamma - 1)\rho e \tag{2}$$

Air was modelled to have an ambient pressure of 101.33 kPa through specifying the adiabatic constant, γ = 1.4, air density, ρ = 1.225 kg/m^3 and initial internal energy, e = 2.068 × 10^5 kJ/kg (Table 2).

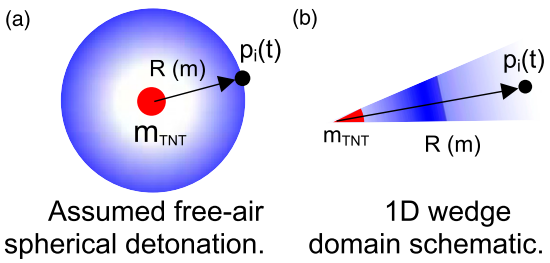

Figure 3. 1D model of the detonation and early-stage blast propagation assuming a spherical free-air detonation (Denny and Clubley, 2019b). (a) Assumed free-air spherical detonation, (b) 1D wedge domain schematic.

Table 2. Equations of state for air and TNT.

	Air	TNT
Equation of state	Ideal gas	JWL
Initial conditions	γ = 1.4 e = 2.068 × 10^5 kJ/kg ρ = 1.225 kg/m^3	A = 3.7377 × 10^5 MPa B = 3.7471 × 10^3 MPa R_1 = 4.15 R_2 = 0.9 ω = 0.35

To model both the detonation of explosive material and subsequent shock wave propagation through air, a multi-material Euler–Godunov solver was specified. A pressure gauge was defined within the wedge domain at a standoff distance of 0.5 m to monitor mesh sensitivity effects and to compare with empirical blast wave calculations (Hyde, 1991; Kingery and Bulmash, 1984).

Sensitivity studies were undertaken to assess the effect of mesh resolution on the blast wave parameters calculated at the 0.5 m standoff distance (see Supplementary Appendix-1D Mesh Sensitivity Study). Following verification, the CFD analysis was performed until the shock front propagated to a standoff distance of 0.5 m, then saved as a remap file (.FIL) to be utilised as initial conditions for subsequent 3D analyses.

Blast wave propagation (R > 0.5m) & structural interaction (3D models). The 3D modelling domain was defined and filled with air modelled as an ideal gas. The 1D model datafile was 'remapped' into the 3D domain using coordinates for the detonation point corresponding to the experimental setup (Figure 1). Again, a multi-material, 3D Euler–Godunov solver was adopted so both air and detonation products were modelled from the remapped 1D analysis data.

The rigid corner was modelled using void cells, forming a cuboid obstacle with dimensions consistent with the experiments (Figure 1). By default, void cells have reflective boundary conditions, thus modelling a perfectly rigid structure with reflective surfaces. Pressure monitoring points were assigned at four locations (A, B1, B2 and B3) in the domain using 3D Cartesian coordinates corresponding to the reference experimental setup (Figure 1). A reflective boundary condition was assigned to the lower z-plane of the domain to model the ground surface, and transmissive 'flow out' boundary conditions were assigned to all other exterior domain boundaries to model free-field (unobstructed) blast wave propagation.

The free-field scenario without the corner structure was modelled by removing the block of void cells. The corner & wall scenario was modelled by specifying a reflective boundary condition to the y = 0 plane, thus representing a rigid wall along the bottom edge of the modelling domain (Figure 2).

As found in other CFD studies (Denny and Clubley, 2019a; Rigby et al., 2014), transmissive boundary conditions were not fully effective, with some localised reflection occurring at the domain sides. Outer dimensions of the 3D domain were therefore made sufficiently large to reduce any potential boundary perturbations from interfering with regions of interest, particularly in the vicinity of pressure gauge locations. An iterative approach was taken during the development of the 3D model to optimise the domain size to provide sufficient space to reduce unwanted boundary interference effects while reducing the computational expense of the modelling problem.

It was observed in preliminary models that pressure histories were sensitive to boundary perturbations at the 'ceiling' of the model (upper z plane). Expansion waves occurring at domain edges are a commonly encountered problem in CFD analyses, see Figure 4 (Rigby, 2014). In this

study, a number of preliminary models were run to determine the domain height required to provide sufficient travel distance such that these expansion waves would not arrive at a gauge location before the model had terminated. The total vertical height of the modelling domain was 2.0 m to allow sufficient space above the detonation plane (z = 1.35 m) to reduce the influence of boundary interference on blast propagation and pressure calculations. Similarly, spacing was required adjacent to gauge locations (0.35 m). Following these observations, the 3D modelling domains comprised exterior dimensions of 1.7 m × 2.75 m × 2.0 m (Figure 1).

Sensitivity studies were undertaken to optimise the mesh size and verify the accuracy and reliability of the 3D model of the corner blast scenario (see Supplementary Appendix-3D Mesh Sensitivity Study). A higher resolution (5 × 5 mm) was specified in the x-y plane to increase accuracy of blast propagation in the lateral direction, while managing computational resource. This maximised accuracy of blast phenomena associated with the primary shock front in the lateral direction between the detonation point and gauges, including reflections at the corner (and wall) surfaces, and subsequent diffraction around the corner. In this study, ground reflections arrived at all gauges after the primary shock front due to their height (1.35 m) above the ground, thus a relatively coarser mesh in the vertical axis was acceptable. Mesh convergence was observed for element dimensions of 5 × 5 × 10 mm, giving rise to a total of 37.7 million elements within the modelling domain.

Following verification and sensitivity studies, all models were specified with consistent setup conditions (i.e. mesh configuration, remap location, material properties and pressure gauge locations) to allow direct comparison between the model results. The 3D CFD models were simulated for a duration of t = 7.0 ms, which allowed sufficient time for the primary blast wavefront to propagate around the corner and pass the furthest measurement location, B3 (Figure 1). Pressure data were extracted from the models at time increments of 0.02 ms, consistent with the experimental data acquisition; this provided adequate resolution of pressure histories while maintaining manageable data storage. Simulations were run on a Dell Alienware Aurora R11 workstation (Intel(R) Core(TM) i9-10900 KF @ 3.70 GHz CPU) with 64 Gb RAM. The 7 ms simulation of the final model with 37.7 million elements required 660 h using 63 Gb RAM and four cores.

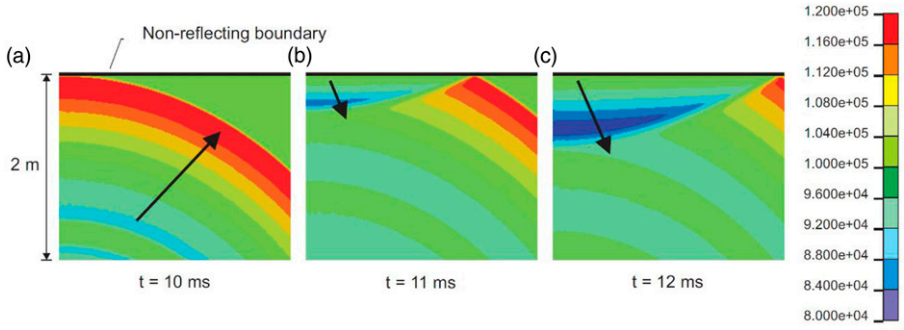

Figure 4. Expansion waves occurring at a non-reflective domain boundary during computational fluid dynamics analysis – contours of pressure (units in Pa) (Rigby, 2014).

Results

Validation of the corner model

Calculated pressure-time histories for each gauge location are plotted in Figure 5 and overlaid with experimental data from Gajewski and Sielicki (2020). As expected, peak overpressures decreased for each subsequent gauge location and at increasing distance around the corner (Figure 5). Decreasing peak pressures are expected with increasing stand-off distance although an enhanced reduction was observed due to shielding from the corner structure.

Calculated peak overpressure and peak specific impulse for each gauge location are plotted in Figure 6 and overlaid with experimental data from Gajewski and Sielicki (2020). Simulated peak overpressures show fair agreement with the experimental data, with magnitudes slightly below the experimental means, although with relatively small absolute differences (Figure 6(a); Table 3). Peak specific impulses demonstrated better agreement with the experimental data (within 5 kPa.ms of mean), although typically exhibited reduced values in comparison to experiments (Figure 6(b); Table 3). It should be noted that there is a large degree of variation in the experimental data obtained by Gajewski and Sielicki (2020). Given this experimental variability, the simulated pressure-time histories, peak overpressures and peak specific impulses were acceptable and exhibited similar trends with respect to different radial stand-off distance and locations surrounding the corner (Figures 5 and 6).

Analysing blast-structure interaction effects on loading

Pressure contours show the primary shock front propagating from the detonation point towards gauge A, which is followed by reflections from the corner structure (Figure 7(a) and (b)) and also from the lower wall in the corner and wall scenario (Figure 7(c) and (d)). Reflections catch-up and gradually merge with the primary shock front (Figure 7(b) and (d)) before diffracting around the corner structure upon reaching the corner vertex. Inspection of pressure contours shows that the diffracted wavefront had decreased pressure with proximity to the shielded corner surface.

The simulated pressure histories were analysed to determine the influence of the corner and the lower wall on the blast loading obtained at each gauge location (using the free-field scenario as a baseline case).

Gauge A. Initial peak overpressures at gauge A were effectively the same ($P_i \approx 175$ kPa) for all modelling scenarios (Table 4). This is expected as gauge A was directly exposed to the unimpeded primary shock front, which is initially unaffected by the presence of the corner or the wall. For the corner scenario and the corner & wall scenario, a second pressure peak occurred ≈0.5 ms after the primary shock front, as visible in Figure 8(b) and (c). Without the wall, this second peak was lower in magnitude than the first one, so its major influence was on the impulse and duration-dependent injury criteria. However, for the corner and wall scenario, this second pressure peak of 270.4 kPa was 53.7% higher than the initial peak pressure (Table 4). Peak specific impulse at gauge A was 38% higher for the corner scenario than the free-field, and 110.3% higher for the corner and wall scenario than the free-field (Table 4). Significantly increased impulse and peak overpressure for the corner and wall scenario is attributed to channelling from the lower wall and corner, which effectively focusses blast reflections at gauge A, as visible in Figure 7.

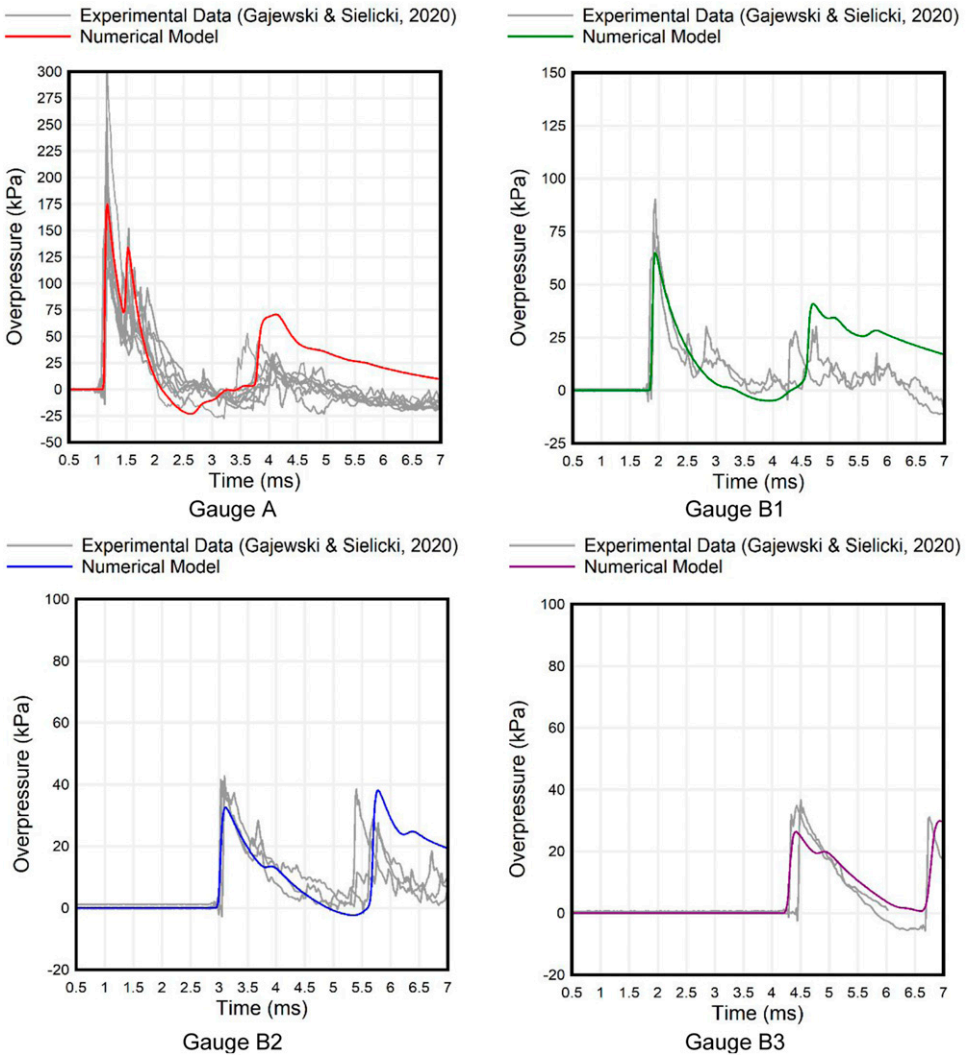

Figure 5. Verifying the corner model with experimental data from (Gajewski and Sielicki, 2020): pressure-time histories at each gauge location.

Gauges B1-B3. Inspection of the overpressure histories at gauges B1-B3 shows that blast interaction with the corner caused a delay in the shock front arrival (Figure 8(d)–(l)). This delay represents the additional time required for the blast wave to diffract around the corner and propagate over a longer distance in comparison to the direct radial distance in the free-field scenario.

For the corner scenario (no wall), blast wave interaction with the corner caused a shielding effect at gauges B1-B3 with significantly reduced peak overpressure and lower peak specific impulse (Table 4). Peak overpressures were reduced by 43%–60% at locations B1-B3 behind the corner in comparison to the free-field scenario (Table 4). Peak specific impulses at gauges B1-B3 were 38%–48% lower (Table 4). Although the corner reduced cumulative and peak specific impulses in comparison to the free-field, the positive phase duration was not notably affected (Figure 8).

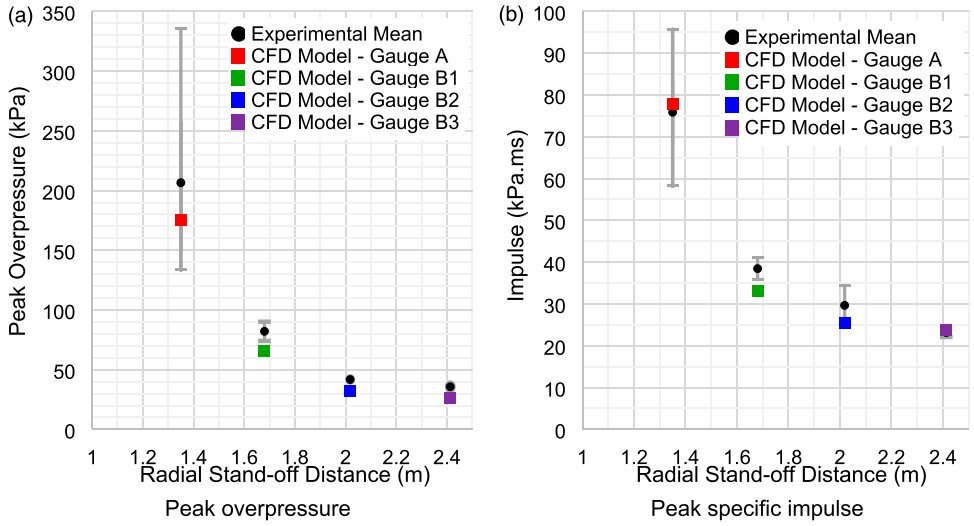

Figure 6. Verifying corner model with experimental data from (Gajewski and Sielicki, 2020): calculated peak overpressure and peak specific impulse at each gauge location. (a) Peak overpressure, (b) Peak specific impulse.

Table 3. Verifying corner model with experimental data from Gajewski and Sielicki (2020): Calculated peak overpressure and peak specific impulse at each gauge location.

	Peak overpressure, P_i (kPa)			Peak specific impulse, I_i (kPa.ms)		
Gauge	Experimental mean	Model	Difference	Experimental mean	Model	Difference
A	206.6 (134.0–335.8)	175.0	31.6	75.9 (58.3–95.7)	77.9	2.0
B1	82.2 (74.1–90.2)	65.6	16.6	38.5 (35.8–41.1)	33.2	5.3
B2	41.8 (41.1–42.7)	32.5	9.3	29.7 (25.8–34.4)	25.5	4.2
B3	35.8 (34.8–36.7)	26.2	9.6	23.2 (22.1–24.2)	24.3	1.1

For the corner and wall scenario, interaction of the primary shock front with the corner caused a similar shielding effect at gauges B1-B3, resulting in effectively the same overpressures as the corner model, with primary peak overpressures significantly reduced (43%–59%) in comparison to the free-field scenario (Table 4). However, channelling from the wall caused a second series of pressure peaks (see Figure 8(f), (i) and (l)) that all exceeded the primary wavefront overpressure in comparison to the corner alone (Table 4). Taking into consideration the maxima of these successive pressure peaks, channelling from the corner and wall reduced the shielding effect of the corner with overpressures at B1-B3 reduced to a lesser extent (0.5–29%) relative to the free-field scenario (Table 4).

Overpressure histories at B1-B3 for the corner and wall scenario demonstrated increasingly complex waveforms featuring multiple pressure peaks with extended positive phase durations, or durations (and impulses) that could not be resolved due to unreasonable computational demand (Figure 8). Importantly, peak specific impulses at gauges A and B1 were 110.3% and 169% higher than the free-field scenario (Table 4). Inspection of pressure histories (Figure 8(f), (i) and (l)),

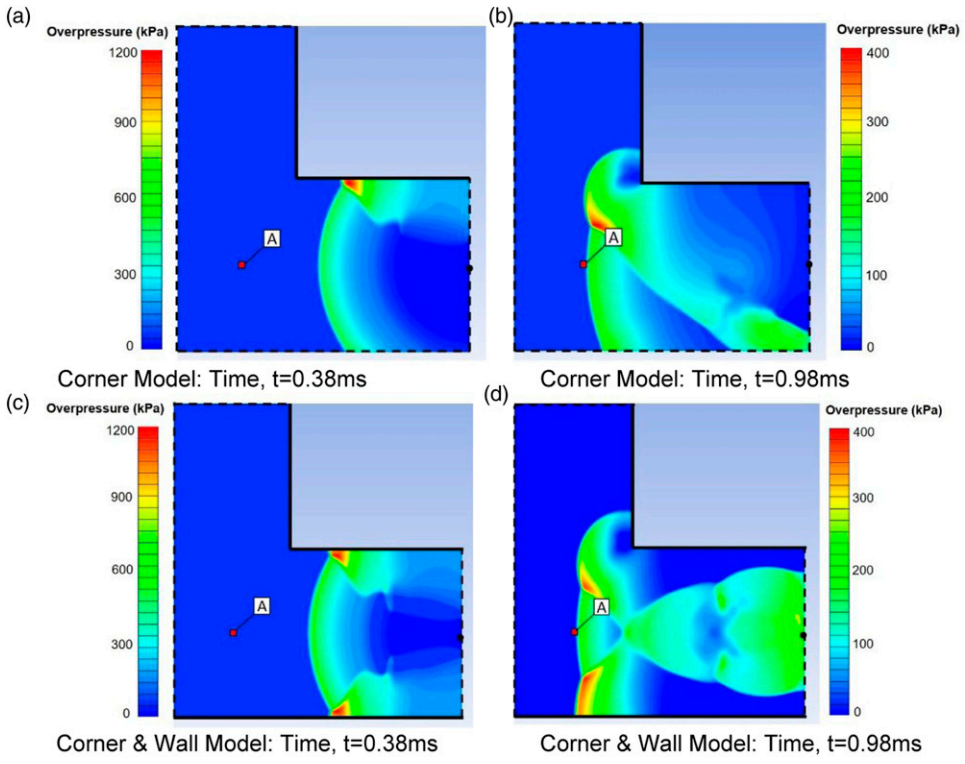

Figure 7. Plan view (z = 1.35 m) of pressure contours at subsequent time intervals showing primary and reflected blast waves approaching gauge A.

confirms that the significantly higher peak specific impulses in the corner & wall scenario are due to the arrival of later-stage overpressures (i.e. ≈2 ms after shock arrival at B1-B3).

Discussion

Blast-structure interaction effect on primary injury risk

For each gauge location, PBI risk was determined by plotting blast wave parameters calculated in each CFD model with pre-defined PBI criteria (Figure 9), adopting the graphical method for PBI prediction as developed by Denny et al. (2021a). Expected PBIs at each gauge location for each blast scenario are summarised in Table 5.

For the free-field and corner scenarios, the risk of PBI at gauge A was identical as simulated peak overpressures and positive phase durations were unaffected at this location. From inspection of Figure 9, blast parameters at gauge A correspond to the threshold conditions for pulmonary (lung) injury and there is over a 50% probability of mild brain haemorrhage and ear drum rupture. The addition of a wall caused a secondary pressure peak (maximum) that, if considered, significantly increased the risk of pulmonary blast injury towards a 1% risk of fatality (Figure 9).

Table 4. Comparing loading parameters between the free-field scenario, the corner and the corner & wall scenarios at each gauge location.

(a) Computed peak overpressures.

		Peak overpressure, P_i (kPa)						
Radial stand-off distance (m)	Gauge	Free-field model	Corner model	% Difference[a]	Corner & Wall model[b]		% Difference[a]	
1.35	A	175.9	175.0	−0.5	176.0	270.4	0.1	53.7
1.68	B1	114.9	65.6	−42.9	65.2	81.6	−43.3	−29.0
2.02	B2	80.5	32.5	−59.6	32.3	70.8	−59.9	−12.0
2.41	B3	61.8	26.2	−57.6	25.8	61.5	−58.2	−0.5

(b) Computed peak specific impulse.

		Peak Specific Impulse, I_i (kPa.ms)				
Radial stand-off distance (m)	Gauge	Free-field model	Corner model	% Difference[a]	Corner & Wall Model	% Difference[a]
1.35	A	56.3	77.9	38.3	118.4	110.3
1.68	B1	53.2	33.2	−37.6	143.1	169.0
2.02	B2	49.9	25.5	−48.8	—[c]	—
2.41	B3	47.1	24.3	−48.4	—[c]	—

[a]% Differences are with respect to free-field scenario.
[b]Pressure histories from the Corner & Wall model exhibited primary and secondary pressure peaks.
[c]Pressure histories were too complex to definitively determine the positive phase duration or peak specific impulse.

For the corner-only scenario, reduced peak overpressures at gauges B1-B3 due to shielding results in lower risk and severity of expected PBIs at all three locations (Figure 9). At gauge B2, for example, the lower peak overpressure reduced the risk of eardrum rupture from almost 50% (free-field scenario) to below the threshold level, thus eardrum injury would no longer be expected (Figure 9). Such shielding effects are believed to have occurred in the 2020 Beirut blast where shielding from the grain silos and other high-rise structures are thought to have mitigated harm (Sawaya, 2021).

For the corner and wall scenario, peak overpressure at B1 is effectively the same as the corner model, although an increased positive phase duration is associated with an increased PBI risk. When the secondary (maximum) pressure peak at B1 is considered (due to channelling caused by the wall), injury risk increases to the threshold for lung injury (Figure 9, Table 5). Injury risk at gauge location B2 and B3 could not be calculated as the blast waveforms were too complex to definitively ascertain the positive phase durations, but it is likely that any increase in duration would adversely affect blast injury risk.

Overall, analysis has shown that in comparison to the free-field scenario, the corner significantly reduced injury risk at B1-B3 (behind the corner) due to shielding. However, the addition of a wall created channelling, which caused secondary and successive pressure peaks with increased magnitude. The higher magnitude pressures significantly increased injury risk at gauge A and reduced the protective shielding effect at gauge locations behind the corner, in comparison to the

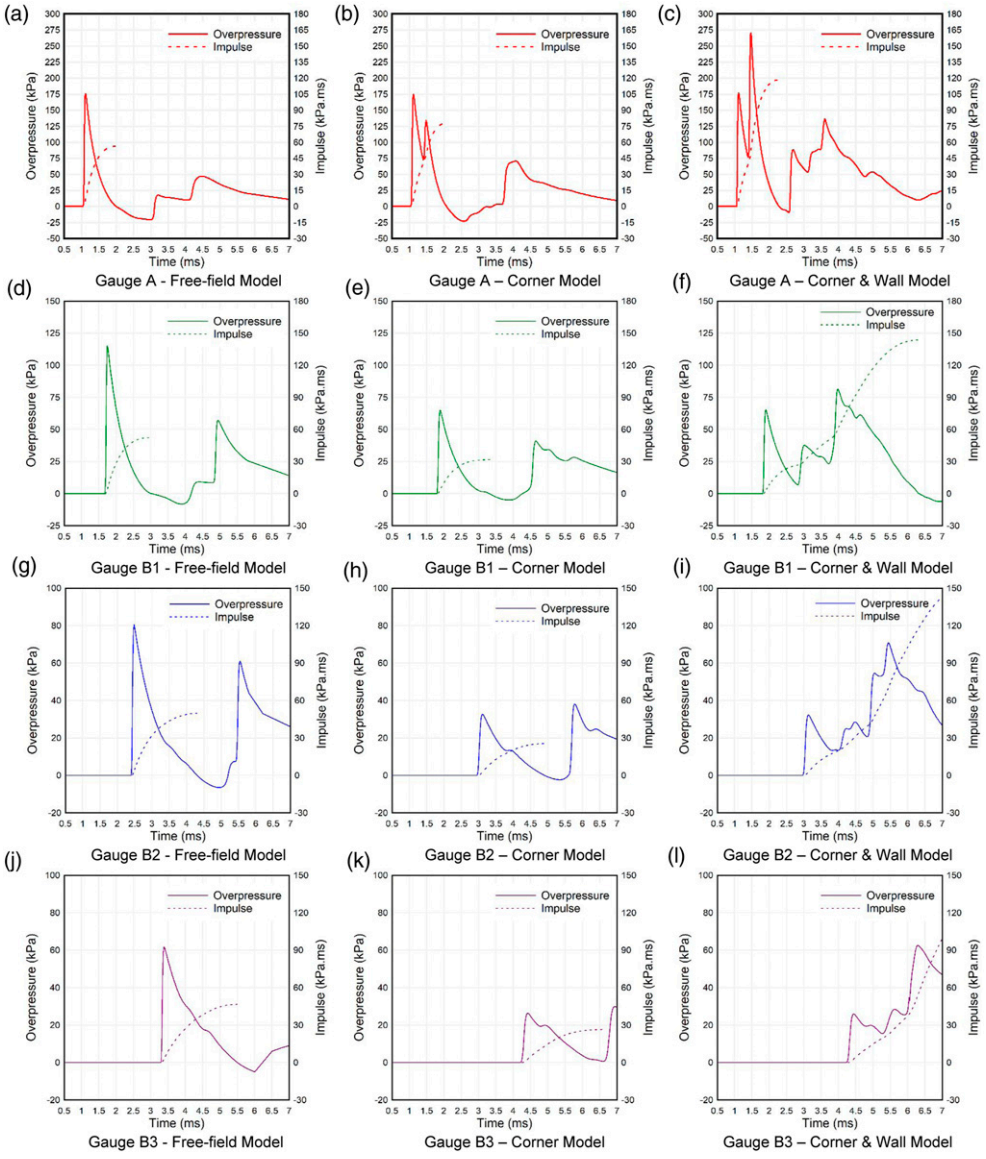

Figure 8. Computational fluid dynamics model overpressure and cumulative impulse histories at each gauge and each blast scenario.

corner alone. While beyond the scope of this study, it is likely that shielding from the corner would also provide protection from fragmentation.

Suitability and limitations of existing PBI criteria

At present, PBI criteria are limited to estimating the likelihood of injury or fatality based on the occurrence of a single blast pressure profile and the loading parameters that would be observed at an

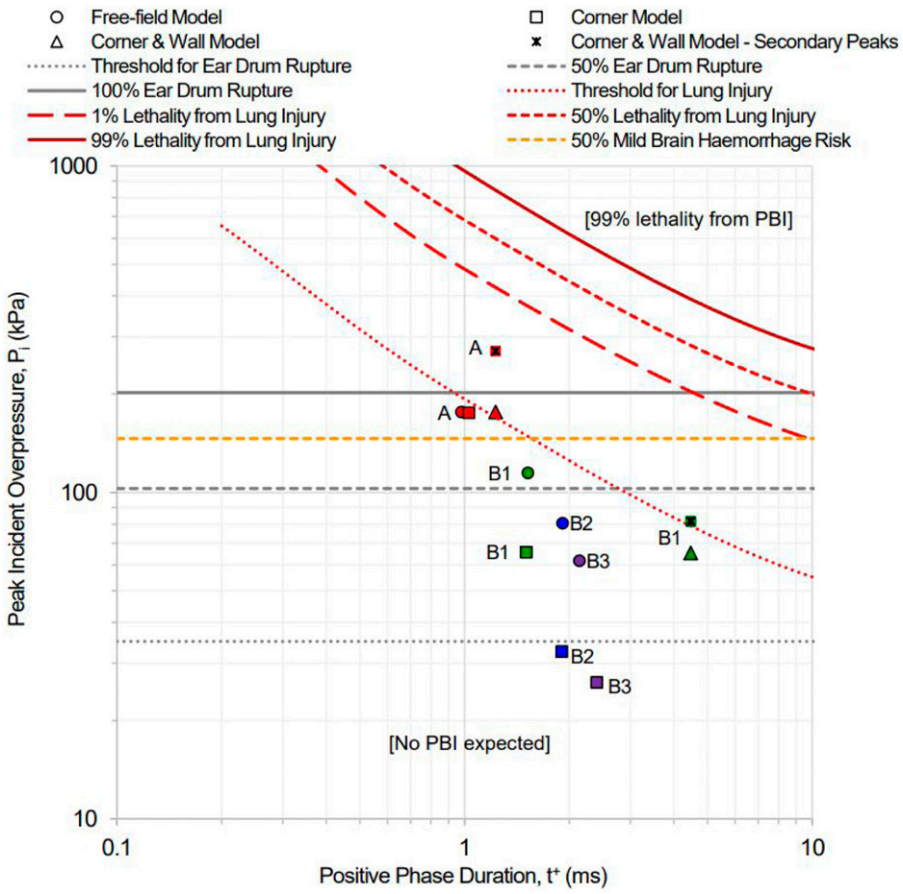

Figure 9. Expected primary blast injury risk (see Table 1) at each gauge location for each blast scenario using blast parameters calculated by computational fluid dynamics models.

unobstructed point in space. Depending on the criteria, input loading conditions are often characterised by the peak overpressure and duration, which may not be appropriate or valid for complex waveforms. Amongst many other limitations, current injury criteria do not account for blast interaction behaviour with the person itself, where the actual loading subjected on a person depends on their geometry and orientation (Needham et al., 2015). Through analysis of individual pressure histories in this study, a range of specific challenges and limitations were identified relating to the suitability of existing injury criteria when applied to complex blast scenarios.

At gauge location A, peak overpressures and positive phase durations remained effectively consistent, however, waveforms measured in the corner scenario and the corner and wall scenario exhibited non-trivial secondary pressure peaks and a 38% and 110% higher peak specific impulse, respectively (Table 4). Although some injury criteria include blast impulse (US DoD, 2008), the majority do not, and typically require inputs of peak overpressure and duration parameters. Importantly, higher impulse represents increased energy and momentum transfer (Rigby et al., 2019), which may influence injury mechanisms and health outcomes. For example, predictive criteria for pulmonary blast (lung) injury (Bowen et al., 1968) demonstrates a clear dependence on both peak

Table 5. Summary of expected primary blast injuries at each gauge location for each blast scenario.

Blast scenario	Expected risk of primary blast injury at each gauge			
	A	B1	B2	B3
Free-field	Near 100% risk of eardrum rupture >50% risk of mild brain haemorrhage Near threshold for lung injury	>50% risk of eardrum rupture	<50% risk of eardrum rupture, but over threshold	<50% risk of eardrum rupture, but over threshold
Corner	As above (same as free-field)	<50% risk of eardrum rupture, but exceeds threshold	No PBIs expected	No PBIs expected
Corner & Wall	As above with: 100% risk of eardrum rupture[a] Near 1% fatality risk from lung injury[a]	As above with: threshold for lung injury[a]	N/A	N/A

PBI: Primary blast injuries.
[a]Taking secondary pressure peaks (maximum overpressure) into account.

overpressure and impulse, where increased impulse is associated with higher probability of fatality. There is also a danger that these complex features of a modified blast waveform (i.e. multiple peaks and increased peak specific impulse) will not be accounted for when using existing injury criteria as they typically only require peak overpressure and duration as input parameters, resulting in unreliable injury predictions.

At gauge A, interaction with the corner caused secondary peak overpressures representing a non-trivial injury risk, or in the case of the corner and wall scenario, a significantly increased injury risk. Even for simple free-field scenarios, analysis of pressure histories in this study demonstrated that ground reflections generated secondary blast waves with peak overpressures associated with injury risk. This raises important questions about how to interpret existing PBI criteria that assume exposure to a single blast wave when secondary and successive peaks in overpressure occur. At present, there is no understanding of the effects of exposure to multiple blast waves on injury, and whether successive exposures are associated with cumulative injury.

As a result, blast waveforms that contain multiple pressure peaks or a positive phase duration that is extended or less clearly defined, such as those found in the corner and wall scenario, present a significant challenge and reduced confidence in predicting injury outcomes. Blast waves at gauges B1-B3 maintained a more ideal waveform following interaction with the corner alone, suggesting that application of injury criteria may be valid and sufficiently reliable in simple scenarios where interaction effects are less.

Current application challenges for urban infrastructure

This work has demonstrated that even for relatively simple urban layouts, corners and walls significantly alter the risk of PBIs, sometimes for the better (corner shielding) and sometimes adversely (e.g. walls due to channelling). There are a near-endless range of possible urban configurations, and each will give rise to a wide range of interaction and loading effects. Importantly,

alternative layouts may magnify loading conditions including increased peak overpressure, stagnation pressures and longer positive phase durations, which are associated with increased injury risk. This study was also limited to the investigation of blast interaction phenomena assuming perfectly rigid structures, neglecting the effects of structural deformation or frangibility, which would also influence loading modification as well as including other types of injuries due to glazing failure or falling debris.

The extent of loading modification following blast interaction with structures therefore depends on the individual scenario, layout and configuration of structures amongst many other factors. With so many variables and potential scenarios, it is challenging to predict the consequences in terms of injury risk and severity without knowledge or fast-running tools to estimate blast loading conditions.

Further research is therefore needed to develop understanding of different urban blast scenarios to determine the sensitivity of different factors and variables (i.e. upper and lower bounds) and the subsequent consequences this has on injury from a probabilistic basis. One of the difficulties in the current work was making reasonable estimates of positive phase duration at locations where the blast load comprised multiple complex waveforms. Further understanding of complex blast loading effects and their influence on blast injury would support the development of more advanced predictive models, inform requirements for protection and improve hazard preparedness.

Conclusions

This study has examined the influence of a rigid corner and a wall on blast loading characteristics and PBI risk. Computational fluid dynamics models demonstrated that the corner reduced peak pressures and impulse at the locations of shielded gauges behind the corner, which corresponded to a significantly reduced risk and severity of PBI. Gauges behind the corner maintained ideal-type waveforms following blast interaction with the corner, suggesting application of PBI criteria remained valid. Adding a wall caused channelling, leading to overall higher pressures and impulse in comparison to the corner alone. Complex waveforms featuring multiple pressure peaks and increased peak specific impulse occurred at the exposed location (gauge A) and gauges B1-B3 which identified specific challenges and reduced reliability for injury prediction.

As CFD blast modelling capabilities continue to advance, this study provides important awareness and understanding of the limitations of using existing injury criteria to predict PBIs. Findings from this study raise awareness for researchers modelling injury risk in urban environments and highlights further areas of research required to improve understanding of complex blast loading conditions on injury risk and outcomes. This work could have potential value to military personnel working in hostile areas but also medical and emergency services accessing zones where an explosion is likely.

Acknowledgements

The authors gratefully acknowledge the technical support from Mr L. Surey.

Declaration of conflicting interests

The author(s) declared no potential conflicts of interest with respect to the research, authorship, and/or publication of this article.

Funding

The author(s) received no financial support for the research, authorship, and/or publication of this article.

ORCID iDs

Jack Denny https://orcid.org/0000-0003-3181-4747
Genevieve Langdon https://orcid.org/0000-0002-0396-9787
Sam Rigby https://orcid.org/0000-0001-6844-3797
Alex Dickinson https://orcid.org/0000-0002-9647-1944
James Batchelor https://orcid.org/0000-0002-5307-552X

Supplemental Material

Supplemental material for this article is available online.

References

Action on Armed Violence (AOAV) (2020) Explosive Violence in 2019. Available at: https://aoav.org.uk/2020/explosive-violence-in-2019/ (accessed 13 March 2022)

Anderson J (2009) *Computational Fluid Dynamics*. JF Wendted (ed). Third edition. Berlin, Germany: Springer Verlag.

ANSYS (2020) AUTODYN. R1. ANSYS. Available at: www.ansys.com (accessed 11 January 2022)

Axelsson H and Yelverton JT (1996) Chest wall velocity as a predictor of nonauditory blast injury in a complex wave environment. *Journal of Trauma* 40(3S): 31S–37S.

Ben-Dor G (2007) *Shock Wave Reflection Phenomena*. Berlin, Germany: Springer.

Bowen IG, Fletcher ER and Richmond DR (1968) *Estimate of Man's Tolerance to the Direct Effects of Air Blast*. Albuqueque, NM: Lovelace Foundation for Medical Education and Research.

Champion HR, Holcomb JB and Young LA (2009) Injuries from explosions: physics, biophysics, pathology, and required research focus. *Journal of Trauma - Injury, Infection and Critical Care* 66(5): 1468–1477. DOI: 10.1097/TA.0b013e3181a27e7f

Chaudhary RK, Mishra S, Chakraborty T, et al. (2019) Vulnerability analysis of tunnel linings under blast loading. *International Journal of Protective Structures* 10(1): 73–94. DOI: 10.1177/2041419618789438

Denny JW and Clubley SK (2019a) Evaluating long-duration blast loads on steel columns using computational fluid dynamics. *Structure and Infrastructure Engineering* 15(11): 1419–1435. DOI: 10.1080/15732479.2019.1599966

Denny JW and Clubley SK (2019b) Investigating the predictive capacity of eulerian CFD to model long-duration blast loads on finite cross-section geometries. *International Journal of Safety and Security Engineering* 9(1): 73–85. DOI: 10.2495/SAFE-V9-N1-73-85

Denny JW, Dickinson AS and Langdon GS (2021a) Defining blast loading 'zones of relevance' for primary blast injury research: a consensus of injury criteria for idealised explosive scenarios. *Medical Engineering and Physics* 93: 83–92. DOI: 10.1016/j.medengphy.2021.05.014

Denny JW, Dickinson AS and Langdon GS (2021b) Guidelines to inform the generation of clinically relevant and realistic blast loading conditions for primary blast injury research. *BMJ Military Health*. Epub ahead of print. DOI: 10.1136/bmjmilitary-2021-001796

Dobratz BM and Crawford PC (1985) *LLNL Explosives Handbook: Properties of Chemical Explosives and Explosives and Explosive Simulants*. Livermore, CA: Lawrence Livermore Lab.

Drazin W (2017) *Blast Propagation and Damage in Urban Topographies*. Cambridge, UK: University of Cambridge.

Friedlander FG (1946) The diffraction of sound pulses. II. Diffraction by an infinite wedge. *Proceedings of the Royal Society of London A: Mathematical, Physical and Engineering Sciences* 186(1006): 344–351. Available at: http://rspa.royalsocietypublishing.org/content/186/1006/344.abstract (accessed 15 March 2022)

Gajewski T and Sielicki PW (2020) Experimental study of blast loading behind a building corner. *Shock Waves* 30: 385–394. DOI: 10.1007/s00193-020-00936-1

Hao H, Hao Y, Li J, et al. (2016) Review of the current practices in blast-resistant analysis and design of concrete structures. *Advances in Structural Engineering* 19(8): 1193–1223. DOI: 10.1177/1369433216656430

Hyde DW (1991) *Conventional Weapons Program (ConWep)*. Vicksburg, MS: US Waterways Experimental Station.

Hyde DW (1992) ConWep: conventional weapons effects (application of TM 5-855-1). Vicksburg, MS: Waterways experiment station, US army corps of enigneers. Available at: https://pdc.usace.army.mil/software/conwep/

Jensen JH and Bonding P (1993) Experimental pressure induced rupture of the tympanic membrane in man. *Acta Oto-Laryngologica* 113(1–2): 62–67. DOI: 10.3109/00016489309135768

Johnson EM, Grahl N, Langenderfer MJ, et al. (2022) An experimental and simulated investigation into the validity of unrestricted blast wave scaling models when applied to transonic flow in complex tunnel environments. *International Journal of Protective Structures*. Epub ahead of print. DOI: 10.1177/20414196221095252

Kingery CN and Bulmash G (1984) *Airblast Parameters from TNT Speherical Air Burst and Hemispherical Surface Burst*. Technical Report ARBRL-TR-02555. Aberdeen Proving Ground, MD: Ballistic Research Laboratories.

Kinney GF and Graham KJ (1985) *Explosive Shocks in Air*. 2nd edition. New York, NY: The Macmillan Company.

Lee EL, Hornig HC and Kury JW (1968) *Adiabatic Expansion of High Explosive Detonation Products*. (Report UCRL-50422). Livermore, CA: University of California Radiation Lab.

Li E, Yoshinaka A and Josey T (2008) Weathervane: a single point model for blast injury approximations. In: 20th Symposium on Military Aspects of Blast and Shock, Oslo, Norway, 1–5 September 2008.

Mays G and Smith P (1995) *Blast Effects on Buildings*. First Edit. Thomas Telford Limited.

Needham CE, Ritzel D, Rule GT, et al. (2015) Blast testing issues and TBI: experimental models that lead to wrong conclusions. *Frontiers in Neurology* 6(72): 1–10. DOI: 10.3389/fneur.2015.00072

Noorpoor Z, Tavangar S, Soury H, et al. (2020) A computational fluid dynamics approach for air blast propagation using OpenFOAM and Becker-Kistiakowsky-Wilson equation of state. *Heliyon* 6(12): e05852. DOI: 10.1016/j.heliyon.2020.e05852

Peters P (2011) Primary blast injury: an intact tympanic membrane does not indicate the lack of a pulmonary blast injury. *Military Medicine* 176: 110–114.

Rafaels KA, Bass CRD, Panzer MB, et al. (2012) Brain injury risk from primary blast. *Journal of Trauma and Acute Care Surgery* 73(4): 895–901. DOI: 10.1097/TA.0b013e31825a760e

Remennikov AM and Rose TA (2005) Modelling blast loads on buildings in complex city geometries. *Computers & Structures* 83(27): 2197–2205. DOI: 10.1016/j.compstruc.2005.04.003

Rigby SE (2014) *Blast Wave Clearing Effects on Finite-Sized Targets Subjected to Explosive Loads*. PhD thesis. Sheffield, UK: The University of Sheffield.

Rigby S.E., Lodge T.J., Alotaibi S, et al. (2020) Preliminary yield estimation of the 2020 Beirut explosion using video footage from social media. *Shock Waves* 30: 671–675. Available at: https://doi.org/10.1007/s00193-020-00970-z

Rigby SE, Tyas A, Bennett T, et al. (2014) A numerical investigation of blast loading and clearing on small targets. *International Journal of Protective Structures* 5(3): 253–274.

Rigby SE, Akintaro OI, Fuller BJ, et al. (2019) Predicting the response of plates subjected to near-field explosions using an energy equivalent impulse. *International Journal of Impact Engineering* 128(January): 24–36. DOI: 10.1016/j.ijimpeng.2019.01.014

Sawaya G (2021) beirut's grain silos: the monolith that shielded the city during 2020's port blast. Available at: https://www.designboom.com/architecture/beiruts-grain-silos-the-monolith-that-shielded-the-city-02-04-2021/(accessed 4 January 2022).

Sherkar P, Whittaker AS and Aref AJ (2010) *Modeling the Effects of Detonations of High Explosives to Inform Blast-Resistant Design*. (Technical Report MCEER-10-0009). Buffalo, NY: University of Buffalo.

Sherkar P, Shin J, Whittaker A, et al. (2016) Influence of charge shape and point of detonation on blast-resistant design. *Journal of Structural Engineering* 142(2): 04015109. DOI: 10.1061/(asce)st.1943-541x.0001371

Smith PD and Hetherington JG (1994) *Blast and Ballistic Loading of Structures*. London, UK: Routledge.

Smith PD and Rose TA (2002) Blast loading and building robustness. *Progress in Structural Engineering and Materials* 4(2): 213–223. DOI: 10.1002/pse.95

Smith PD and Rose TA (2006) Blast wave propagation in city streets - an overview. *Progress in Structural Engineering and Materials* 8(1): 16–28. DOI: 10.1002/pse.209

Teland JA (2012) *Review of Blast Injury Prediction Models*. Kjeller, Norway: FFI-rappor. Norwegian Defence Research Establishment (FFI).

US Department of Defense (DoD) (2006) *DoD Directive 6025.21E: Medical Research for Prevention, Mitigation, and Treatment of Blast Injuries*. Washington, DC: US Department of Defense

US Department of Defense (DoD) (2008) *UFC 3-340-02, 'Structures to Resist the Effects of Accidental Explosions'*. Unified Facilities Criteria (UFC) 3-340-02. Washington, DC: US Department of Defense.

Valsamos G, Larcher M and Casadei F (2021) Beirut explosion 2020: a case study for a large-scale urban blast simulation. *Safety Science* 137: 105190. DOI: 10.1016/j.ssci.2021.105190